nature machine intelligence

ARTICLES

https://doi.org/10.1038/s42256-020-00263-1

A soft robot that adapts to environments through shape change

Dylan S. Shah[1,3], Joshua P. Powers[2,3], Liana G. Tilton[1], Sam Kriegman[2], Josh Bongard[2] and Rebecca Kramer-Bottiglio[1]✉

Many organisms, including various species of spiders and caterpillars, change their shape to switch gaits and adapt to different environments. Recent technological advances, ranging from stretchable circuits to highly deformable soft robots, have begun to make shape-changing robots a possibility. However, it is currently unclear how and when shape change should occur, and what capabilities could be gained, leading to a wide range of unsolved design and control problems. To begin addressing these questions, here we simulate, design and build a soft robot that utilizes shape change to achieve locomotion over both a flat and inclined surface. Modelling this robot in simulation, we explore its capabilities in two environments and demonstrate the automated discovery of environment-specific shapes and gaits that successfully transfer to the physical hardware. We found that the shape-changing robot traverses these environments better than an equivalent but non-morphing robot, in simulation and reality.

Nature provides several examples of organisms that utilize shape change as a means of operating in challenging, dynamic environments. For example, the spider *Araneus rechenbergi*[1,2] and the caterpillar of the mother-of-pearl moth (*Pleurotya ruralis*)[3] transition from walking gaits to rolling in an attempt to escape predation. Across larger timescales, caterpillar-to-butterfly metamorphosis enables land-to-air transitions, while mobile to sessile metamorphosis, as observed in sea squirts, is accompanied by radical morphological change. Inspired by such change, engineers have created caterpillar-like rolling[4], modular[5–7], tensegrity[8,9], plant-like growing[10] and origami[11,12] robots that are capable of some degree of shape change. However, progress towards robots that dynamically adapt their resting shape to attain different modes of locomotion is still limited. Further, design of such robots and their controllers is still a manually intensive process.

Despite the growing recognition of the importance of morphology and embodiment on enabling intelligent behaviour in robots[13], most previous studies have approached the challenge of operating in multiple environments primarily through the design of appropriate control strategies. For example, engineers have created robots that can adapt their gaits to locomote over different types of terrain[14–16], transition from water to land[17,18] and transition from air to ground[19–21]. Other research has considered how control policies should change in response to changing loading conditions[22,23], or where the robot's body was damaged[24–26]. Algorithms have also been proposed to exploit gait changes that result from changing the relative location of modules and actuators[27], or tuning mechanical parameters, such as stiffness[28]. In such approaches, the resting dimensions of the robot's components remained constant. These robots could not, for instance, actively switch their body shape between a quadrupedal form and a rolling-optimized shape.

The emerging field of soft robotics holds promise for building shape-changing machines[29]. For example, one robot switched between spherical and cylindrical shapes using an external magnetic field, which could potentially be useful for navigating internal organs such as the oesophagus and stomach[30]. Robotic skins wrapped around sculptable materials were shown to morph between radially symmetric shapes such as cylinders and dumbbells to use shape change as a way to avoid obstacles[31]. Lee et al. proposed a hybrid soft–hard robot that could enlarge its wheels and climb onto step-like platforms[32]. A simulated soft robot was evolved to automatically regain locomotion capability after unanticipated damage, by deforming the shape of its remnant structure[33]. With the exception of the study by Kriegman et al.[33], control strategies and metamorphosis were manually programmed into the robots, thereby limiting such robots to shapes and controllers that human intuition is capable of designing. However, there may exist non-intuitive shape–behaviour pairings that yield improved task performance in a given environment. Furthermore, manufacturing physical robots is time consuming and expensive relative to robot simulators such as VoxCad[34], yet discovering viable shape–behaviour pairs and transferring simulated robots to functioning physical hardware remains a challenge. Although many simulation-to-reality ('sim2real') methods have been reported[24,25,35–43], none have documented the transfer from simulation to reality of shape-changing robots.

To test whether situations exist where shape change improves a robot's overall average locomotion speed within a set of environments more effectively than control adaptations, here we present a robot that actively controls its shape to locomote in two different environments: flat and inclined surfaces (Fig. 1). The robot had an internal bladder, which it could inflate/deflate to change shape, and a single set of external inflatable bladders that could be used for locomotion. Depending on the core's shape, the actuators created different motions, which could allow the robot to develop new gaits and gain access to additional environments. Within a soft multi-material simulator, an iterative 'hill-climbing' algorithm[44] generated multiple shapes and controllers for the robot, then automatically modified the robots' shapes and controllers to discover new locomotion strategies. No shape–controller pairs were found that could locomote efficiently in both environments. However, even relatively small changes in shape could be paired with control policy adaptations to achieve locomotion within the two environments. In flat and even

[1]Department of Mechanical Engineering and Materials Science, Yale University, New Haven, CT, USA. [2]Department of Computer Science, University of Vermont, Burlington, VT, USA. [3]These authors contributed equally: Dylan S. Shah, Joshua P. Powers. ✉e-mail: rebecca.kramer@yale.edu

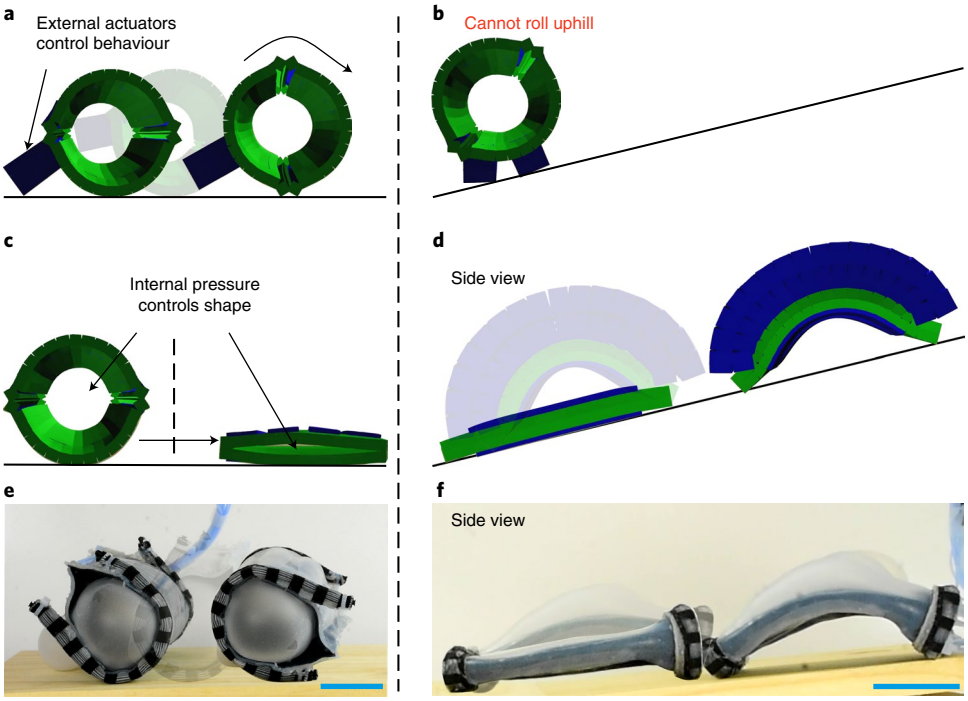

Fig. 1 | Shape change can result in faster locomotion speeds than control adaptation, when a robot must operate in multiple environments. a, Using inflatable external bladders, rolling was the most effective gait on flat ground. **b**, Rolling was ineffective on the inclined surface. **c**,**d**, Search discovered a flat shape (achieved by deflating the inner bladder; **c**) and crawling gait (**d**) that allowed the robot to succeed in this environment. **e**,**f**, After discovering these strategies in simulation, we transferred learned strategies for rolling (**e**) and inchworm motion (**f**) to real hardware. Scale bars, 5 cm.

slightly inclined environments, the robot's fastest strategy was to inflate and roll. At slopes above a critical transition angle, the robot could increase its speed by flattening to exhibit an inchworm gait. A physical robot was then designed and manufactured to achieve similar shape-changing ability and gaits (Fig. 2). When placed in real-world analogues of the two simulated environments, the physical robot was able to change shape to locomote with two distinct environmentally effective gaits, demonstrating that shape change is a physically realistic adaptation strategy for robots.

This work points towards the creation of a pipeline that takes as input a desired objective within specified environments, automatically searches in simulation for appropriate shape and control policy pairs for each environment, and then searches for transformations between the most successful shapes. If transformations between successful shapes can be be found, those shape–behaviour pairs are output as instructions for designing the metamorphosing physical machine. In this Article, we demonstrate that at least some shape–behaviour pairs, as well as changes between shapes, can be transferred to reality. Thus, this work represents an important step towards an end-to-end pipeline for shape-changing soft robots that meet the demands of dynamic, real-world environments.

Results

The simulated robot. We initially sought to automate search for efficient robot shapes and control policies in simulation, to test our hypothesis that shape and controller adaptation can improve locomotion speeds across changing environments more effectively when given a fixed amount of computational resources, compared with controller adaption only. To verify that multiple locomotion gaits were possible with the proposed robot design, we first used our intuition to create two hand-designed shape and control policies: one for rolling while inflated in a cylindrical shape (Fig. 1a), and the other for inchworm motion while flattened (Fig. 1d). Briefly, the rolling gait consisted of inflating the trailing-edge bladder to tip the robot forward, then inflating one actuator at a time in sequence. The hand-designed 'inchworm' gait consisted of inflating the four upward-facing bladders simultaneously to bend the robot in an arc. We then performed three pairs of experiments in simulation. Within each pair, the first experiment automatically sought robot parameters for flat ground; the second experiment sought parameters for the inclined plane. Each successive pair of experiments allowed the optimization routine to control an additional set of the robot's parameters, allowing us to measure the marginal benefit of adapting each parameter set when given identical computational resources (summarized in Table 1 and Fig. 3). The three free parameter sets of our shape-changing robot are shape, orientation relative to the contour (equal elevation) lines of the environment, and control policy (Fig. 3a). This sequence of experiments sought to determine whether optimization could find successful parameter sets in a high-dimensional search space, while also attempting to determine to what degree shape change was necessary and beneficial.

In all experiments, fitness was defined as the average speed the robot (measured in body lengths per second ($BL\,s^{-1}$)) attained over flat ground or uphill, depending on the current environment of interest, during a fixed period of time. Parameters for the simulation were initialized based on observations of previous robots[31,45] and adjusted to reduce the simulation-to-reality gap after preliminary tests with physical hardware (see Methods for additional details). The results reported here are for the final simulations that led to the functional physically realized robot and gaits.

In the first pair of experiments, we sought to discover whether optimization could find any viable controllers within a constrained optimization space, which was known to contain the viable hand-designed controllers. Solving this initial challenge served to test the pipeline before attempting to search in the full search space, which has the potential to have more local minima. The shape and orientation were fixed (flat and oriented length-wise, $\theta = 90°$, for the inclined surface, cylindrical and oriented width-wise, $\theta = 0°$ for

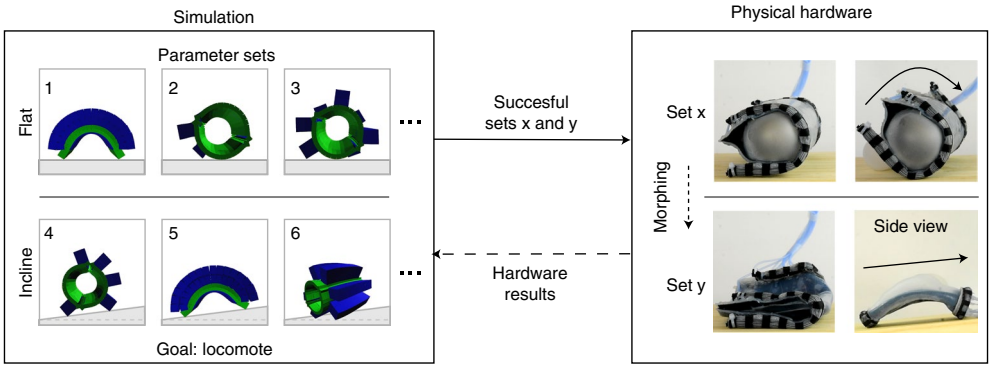

Fig. 2 | Simulation revealed successful shapes and controllers, which we attempted to realize in hardware. Sets consisting of a shape, an orientation and a controller were generated for the robot in simulation. Each numbered sub-panel depicts a single automatically generated parameter set. After running simulations to determine the speed of each set, some were deemed too slow, while successful (relatively quick) sets were used to design a single physical robot that could reproduce the shapes and gaits found in simulation for both environments. During prototyping, actuator limits were measured and incorporated into the simulator to improve the accuracy of the simulation.

Table 1 | Simulation results, reported as the mean and maximum velocity attained for each test condition

Free parameters	Flat ground		Hill		
	Mean	Maximum	Mean	Maximum	Combined maximum
Orientation, shape, control	0.112	0.229	0.026	0.042	0.136
Shape, control	0.112	0.230	0.019	0.025	0.1275
Control	0.114	0.202	0.010	0.023	0.112
Hand-designed rolling	NA	0.203	NA	−0.599	−0.198
Hand-designed inching	NA	0.093	NA	0.065	0.079

The simulator is deterministic, so no mean is reported for the hand-designed gaits (as they will always yield identical locomotion speed). Shape change allowed the robot to switch between dissimilar locomotion gaits, outperforming the benchmark policies. Combined maximum was determined by averaging the maximum speed attainable in both environments. All values have units of body lengths per second (BL s^{-1}).

the flat surface). In the second pair of experiments, the algorithm was allowed to simultaneously search for an optimal shape and controller pair. Finally, in the third pair of experiments, all three parameter sets were open to optimization in both environments, allowing optimization the maximum freedom to produce novel shapes, orientations and controllers for locomoting in the two different environments. For each experiment, we ran 60 independent 'hill climbers' (instantiations of the hill-climbing search algorithm[44], not to be confused with a robot that climbs a hill) for 200 generations, thus resulting in identical resource allocation for each experiment (Fig. 3b,c). In addition, we ran a control experiment in which we fixed the shape of the robot to be fully inflated and oriented width-wise ($\theta = 0°$) for the inclined surface, to determine whether shape change was necessary. The best the robot could do was prevent itself from rolling backward, and it attained a fitness value of −0.001 BL s^{-1}.

When shape and orientation were set as fixed parameters, optimization found a control policy that had a similar behaviour to the hand-designed control policies. Rolling was successful on flat ground (maximum fitness 0.202 BL s^{-1}), and performing inchworm motion was the most effective gait discovered over inclined ground (maximum fitness 0.023 BL s^{-1}), confirming that successful controllers could be found with the proposed pipeline (Table 1). For reference, other robots that exclusively utilize inchworm gaits have widely varied speeds, ranging from 0.013 BL s^{-1} (for a 226-mm-long robot)[46] to 0.16 BL s^{-1} (for a centimetre-scale robot)[47].

For the second pair of experiments (orientation fixed), the best robots produced inflated shapes that rolled over flat ground (max fitness 0.230 BL s^{-1}) and flat shapes that performed inchworm motion on the inclined ground (maximum fitness 0.025 BL s^{-1}). The increased complexity of the search space caused by allowing shape change did not hinder the search process, allowing the algorithm to discover efficient solutions without any a priori knowledge of the viability of the attainable shape–controller pairs.

In the last pair of experiments (all parameters open), the algorithm again discovered that cylindrical rolling robots were the most effective over a flat surface. However, over the inclined surface, the optimization algorithm found better designs with a semi-inflated shape capable of shuffling up the hill when oriented at an angle (maximum fitness 0.042 BL s^{-1}). Using this strategy, the robot achieved combined locomotion of 0.136 BL s^{-1}, outperforming the hand-designed strategy of using crawling on inclines and rolling on flat ground. The deflated shape increased the surface area of the robot in contact with the ground, increasing friction between the robot and the ground, while the non-standard orientation reduced the amount of gravitational force opposing the direction of motion, thereby requiring less propulsive force and reducing the likelihood of the robot rolling back down the hill. However, when we attempted to replicate this behaviour in physical hardware, the robot could not shuffle, and rather rocked in place. Thus, the best transferable strategy for moving up the incline was to attain the flattened shape and traverse the hill using an inchworm-like gait. In all the experiments, the policies found were less finely tuned than those that were hand-designed. Thus, even though optimization produced similar overall behaviours and performance (inching and rolling), these behaviours also included occasional counterproductive or superfluous actuations (Supplementary Video 1). Such unhelpful motions could probably be overcome via further optimization and by adding a fitness penalty for the number of actuators used per time step.

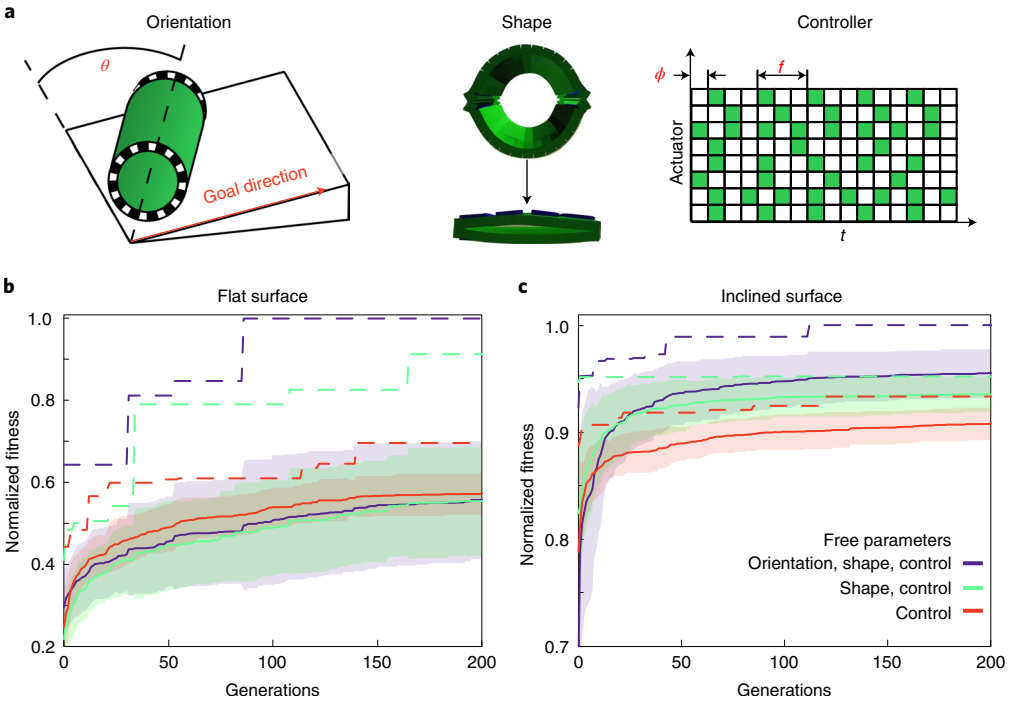

Fig. 3 | Automated search discovered increasingly successful gaits in both environments. a, For each simulation, the algorithm could adjust the orientation, shape and/or controller of the robot. Orientation (θ) was measured by the angle between the robot's leading edge and a constant-elevation line on the surface. Shape was parameterized as the inner bladder's pressure, resulting in a family of shapes between the cylinder and flat shape shown. Control of each actuator was parameterized as the number of timesteps (t) until its first actuation (ϕ) and the number of timesteps between actuations (f). Here we show an example controller for the eight main bladders, with green shaded squares illustrating inflation and white squares showing deflation. **b**,**c**, Results on a flat surface (**b**) and on an inclined surface (**c**). Shaded regions represent 1 s.d. about the mean (solid line) and dashed lines represent maximum fitness. The legend indicates which parameters were to open to optimization, the others being held constant.

Our control experiment, where the robot was constrained to be oriented width-wise against the inclined surface and fully inflated, tested whether optimization could find a way to move up the hill without changing shape, thereby determining whether shape change was necessary to move up the inclined surface at all. Here the most successful of the discovered policies exploited the simulator in ways similar to the physically infeasible robots in the previous experiment, and shuffled uphill. Thus, there were no transferable strategies that allowed locomotion uphill in the control experiment. We ran a Welch's t-test comparing the solutions found through optimization during the three previous pairs of experiments against the transferable solutions in this experiment. The optimized solutions were found to be significantly better, $P<0.05$, providing strong evidence of the necessity of shape change and showing that increasing the dimensionality of the search space helped, rather than hindered, the optimization algorithm.

A similar trend is shown in Fig. 3b,c, where the best robot for each environment was discovered by the pair of experiments in which the hill-climbing algorithm had the most control over the optimization of the robot (increase in maximum fitness of 13.6% over flat ground, 78.9% on the incline), despite the larger number of trainable parameters, and thus an increased likelihood of getting stuck in a local minimum. In addition, the population of simulated robots continued to exhibit similar (and often superior) mean performance compared with the control-only experiments (Fig. 3). These observations suggest that the robots avoided local minima, and that more parameters should be mutable during automated design of shape-changing robots. We hypothesize that maximizing the algorithm's design freedom would be even more important when designing robots with increased degrees of freedom, using more sophisticated optimization algorithms that can operate in an exponentially growing search space.

While optimization found intuitive shapes and behaviours for the given environments (rolling on flat ground, inching on moderate inclines), we further sought to discover optimal shape–behaviour pairs in very slightly inclined environments, where it was not obvious whether the robot would favour rolling or inching. We thus relied on evolution to discover where shape and behavioural transitions should occur across an incline sweep, and whether a gradually changing environment should require a correspondingly gradual change in robot shape. A state-of-the art evolutionary algorithm (distance-weighted exponential natural evolutionary strategies, or DX-NES[48]; see Methods for further details) revealed that gradual changes are not advantageous. Instead, the simulated robot switched between a relatively inflated and deflated core, with a corresponding switch between rolling and inching gaits, at a critical incline angle of 2.5° (Fig. 4). This result suggests that the fitness landscape of shape-changing robots may not be smooth, and that the optimal shape and gait of a robot can be sensitive to slight environmental changes (for example, when the incline angle is just below or just above the critical incline angle). Robots might therefore benefit from being able to detect sudden decreases in performance to allow them to respond by transitioning to a different, more appropriate shape–policy strategy. We further note that the exact critical incline angle, or transition angle, is dependent on the friction between the robot and the surface it is traversing.

Overall, this sequence of experiments showed that automated search could discover physically realistic shapes and controllers for our shape-changing robot in a given environment (a prescribed ground incline). In addition, when faced with an incline sweep, evolutionary algorithms could discover the transition point where shape change is necessary. Although the hand-designed controllers each performed comparably to the best discovered controllers

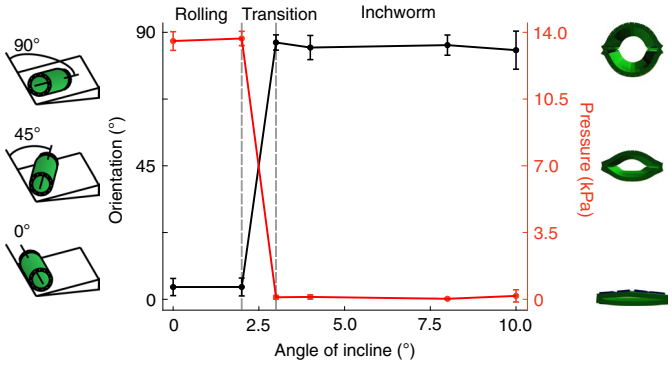

Fig. 4 | Optimal orientation and pressure found in simulation, as a function of the angle of incline. Between 2° and 3°, the best robots switch from being inflated with rolling-like gaits, to deflated with inchworm-like gaits. Error bars represent 1 s.d. over 11 evolutionary trials.

in a single environment, by changing shape, the robot had a better combined average speed in both environments. Concretely, the best shape–controller pair found by hill climbing locomoted at a speed of 0.229 BL s^{-1} on flat ground and 0.042 BL s^{-1} on incline, resulting in an average speed across the two environments of 0.136 BL s^{-1}, compared with the average speed of −0.198 BL s^{-1} for the round shape with a rolling gait and 0.079 BL s^{-1} for the flat shape with an inchworm gait (Table 1).

Transferring to a physical robot. Transferring simulated robots to reality introduces many challenges. For perfect transferal, the simulation and hardware need to have matching characteristics, including: material properties, friction modelling, actuation mechanisms, shape, geometric constraints and range of motion. In practice, hardware and software limitations preclude perfect transferal, so domain knowledge must be used to achieve a compromise between competing discrepancies. Here we sought to maximize the transferal of useful behaviour, rather than strictly transferring all parameters. In simulation, we found that the same actuators could be used to create different locomotion gaits. When restricted to the cylindrical shape, successful controllers typically used sequential inflation of the bladders to induce rolling. The flatter robots employed their actuators to locomote with inchworm motion. To transfer such shape change and gaits to a physical robot, we created a robot that had an inflatable core, eight pneumatic surface-based actuators for generating motion and variable-friction feet on each edge to selectively grip the environment (Fig. 1). This suite of features allowed the robot to mirror the simulated robot's gaits, including rolling and inching. The 'hand-designed controllers' from simulation were transferred to reality by sending the same command sequence from a PC to digital pressure regulators[49] that inflated the bladders, resulting in forward motion. However, it was found that different bladders expanded at different rates and had slightly different maximum inflation before failure, so in the experiments shown in this manuscript, the robots were manually teleoperated to approximate the hand-designed controllers with non-uniform timesteps between each actuation state. Further details on the robot hardware are presented in Methods.

Mirroring simulation, rolling was achieved by inflating the trailing-edge bladder to push the robot forward, exposing new bladders that were then inflated one at a time, sequentially (Fig. 1a and Fig. 5a). Each inflation shifted the robot's centre of mass forward so the robot tipped in the desired direction, allowing the robot to roll repeatedly. This motion was effective for locomoting over flat ground (average speed 0.05 BL s^{-1}). When we attempted to command the robot to roll up inclines, the slope of the incline and the robot's seam made it difficult for the robot to roll. These observations suggest the existence of a transition regime on the physical robot, where the ideal shape–locomotion pair switches from a rolling cylinder to a flat shape with inchworm gait, similar to the simulated robot. However, the boundary is not cleanly defined on the physical hardware: at increasing inflation levels approaching the strain limit of the silicone, the robot could roll up increasingly steep inclines up to ~9°. After just a few such cycles, the bladders would irreversibly rupture, causing the robot to roll backward to the start of the incline.

By accessing multiple shapes and corresponding locomotion modes, shape-changing robots can potentially operate within multiple sets of environments. For example, when our robot encountered inclines, it could switch shapes (Fig. 5a–c and Supplementary Video 1). To transition to a flattened state capable of inchworm motion, the robot would deflate its inner bladder, going from a diameter of 7 cm (width-to-thickness ratio $\gamma = 1$) to an outer height of ~1.2 cm ($\gamma \approx 8.3$) (Fig. 5b). The central portions of the robot flatten to ~7 mm, which is approximately the thickness of the robot's materials, resulting in $\gamma \approx 14$. During controlled tests, an average flat-to-cylinder morphing operation at 50 kPa took 11.5 s, while flattening with a vacuum (−80 kPa) took 4.7 s (see Methods for additional details).

Flattening reduced the second moment of area of the robot's cross-section, allowing the bladders' inflation to bend the robot in an arc (Fig. 5c). At a first approximation, body curvature is given as $\kappa = \frac{M}{EI}$, where M is the externally induced moment, E is the effective modulus and I is the axial cross-section's second moment of area. Thus, flatter robots should bend to higher curvatures for a given pressure. However, even for the flattest shape, bending was insufficient to produce locomotion: on prototypes with unbiased frictional properties, bending made the robot curl and flatten in place.

Variable-friction 'feet' were integrated onto both ends of the robot and actuated one at a time to alternate between gripping in front of the robot and at its back, allowing the robot to inch forward (average speed of 0.01 BL s^{-1} on flat wood). The feet consisted of a latex balloon inside unidirectionally stretchable silicone lamina[50], wrapped with cotton broadcloth. When the inner latex balloon was uninflated (−80 kPa), the silicone lamina was pulled into its fabric sheath, thus the fabric was the primary contact with the ground. When the balloon was inflated (50 kPa), it pushed the silicone lamina outward and created a higher-friction contact with the ground (Fig. 6a). To derive coefficients of static friction (μ) for both the uninflated (μ_u) and the inflated (μ_i) cases, we slid the robot over various surfaces including acrylic, wood and gravel. As the robot slid over a surface, it would typically exhibit an initial linear regime corresponding to pre-slip deformation of the feet, followed by slip and a second linear kinetic friction regime (Fig. 6b). From the pre-slip regime, we infer that on a wood surface $\mu_u = 0.56$ and $\mu_i = 0.70$—an increase of ~25% (Fig. 6c). On acrylic, $\mu_u = 0.38$ and $\mu_i = 0.51$, which is an increase of 35%, yielding an inching speed of 0.007 BL s^{-1}. When the difference in friction ($\Delta\mu = \mu_i - \mu_u$) for the variable-friction feet was too low (such as on gravel), inchworm motion was ineffective, as predicted by simulation (Fig. 6d). Similarly, when the average friction ($\mu_m = (\mu_i + \mu_u)/2$) was too high, it would overpower the actuators and lead to negligible motion (Fig. 6e). On wood, the inchworm gait was effective on inclines up to ~14°, at a speed of 0.008 BL s^{-1} (Fig. 5 and the Supplementary Video 1). Thus, the robot could quickly roll over flat terrain (0.05 BL s^{-1}) then flatten to ascend moderate inclines, attaining its goal of maximizing total travelled distance.

Discussion

In this study, we tested the hypothesis that adapting the shape of a robot, as well as its control policy, can yield faster locomotion across environmental transitions than adapting only the control policy of a single-shape robot. In simulation, we found that a shape-changing robot traversed two test environments faster than an equivalent but

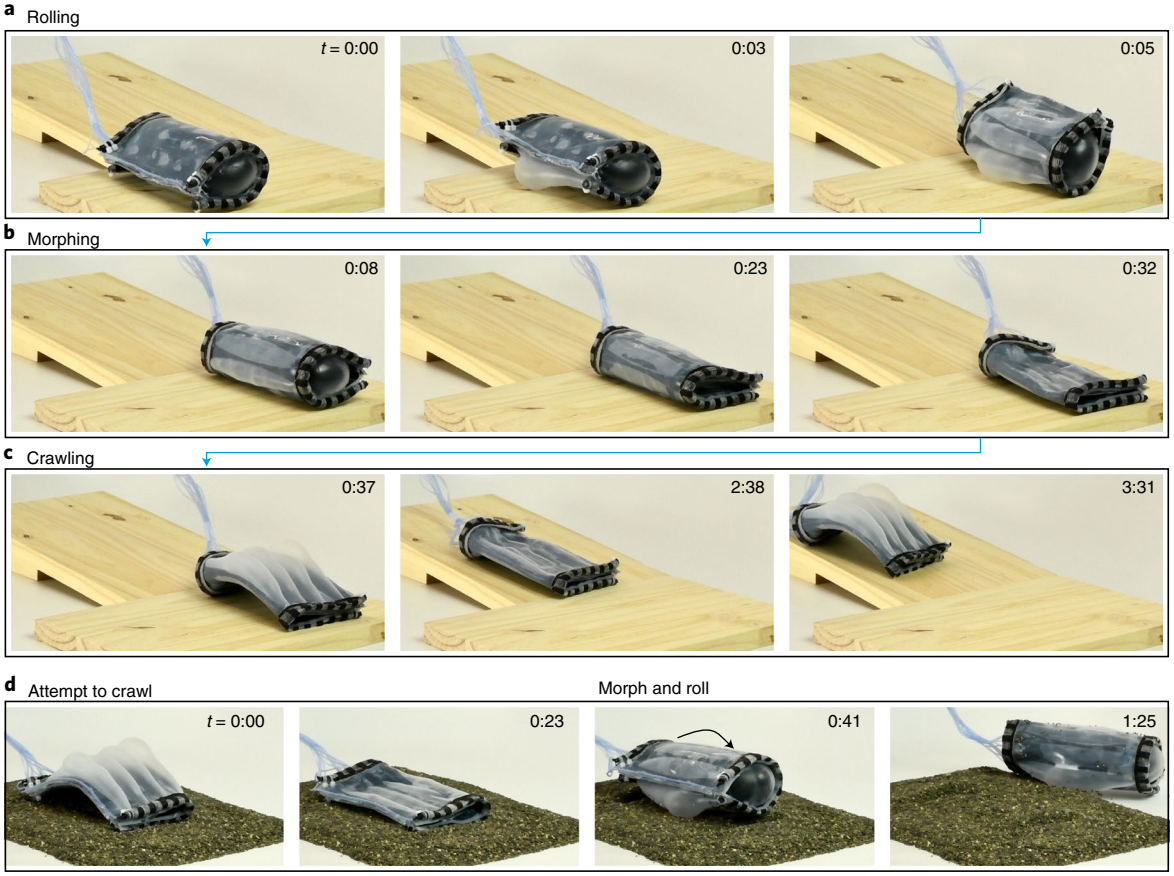

Fig. 5 | Shape change allowed the physical robot to operate in previously inaccessible environments. a, When round, the robot's actuators created a rolling gait that was effective on flat ground. **b**, By deflating its inner bladder, the robot could flatten. **c**, When flat, the outer bladders induced an inchworm-like gait, allowing the robot to ascend inclines up to ~14°. **d**, The inchworm gait gripped the ground to crawl forward, making it ineffective on granular surfaces. When faced with such a situation, the robot could expand its inner bladder to begin rolling. For length-scale reference, the robot is 10 cm by 15 cm when flattened, and 7 cm diameter by 15 cm when round. Times are given in the format of minutes:seconds. Panels **a**–**c** correspond to times from a single trial, while panel **d** is from a different trial and has a separate start time.

non-morphing robot. Then, we designed a physical robot to utilize the design insights discovered through the simulation, and found that shape change was a viable and physically realizable strategy for increasing the robot's locomotion speed. We have also shown progress towards an automated sim2real framework for realizing metamorphosing soft robots capable of operating in different environments. In such a pipeline, simulated shape-changing robots would be designed to achieve a desired function in multiple environments, then transferred to physical robots that could attain similar shapes and behaviours. We demonstrated each component of the pipeline on a representative task and set of environments: locomotion over flat ground and an incline. Starting with an initial robot design, the search method sought valid shapes and control policies that could succeed in each environment. The effective shapes and gaits were then transferred to physical hardware. However, the simulation was able to generate some non-transferable behaviour by exploiting inaccuracies of some simulation parameters. For example, when the friction coefficient was too low, the robot would make unrealistic motions such as sliding over the ground. Other parameters, such as modulus, timescale, maximum inner bladder pressure, resolution of the voxel simulation (that is, the number of simulated voxels per bladder) and material density, could be adjusted without causing drastic changes in behaviour. Developing a unified framework for predicting the sim2real transferability of multiple shapes and behaviours to a single robot remains an unsolved problem.

Insights from early physical prototypes were used to improve the simulator's hyperparameters (such as physical constants), resulting in more effective sim2real transferal. Pairing hardware advances with multiple cycles through the sim2real pipeline, we plan to systematically close the loop such that data generated by the physical robot can be used to train a more accurate simulator, after which a new round of sim2real transfers can be attempted. This iterative process will be used to reduce the gap between simulation and reality in future experiments.

With advances such as increased control of the physical robots' shape and more efficient, parallelized soft-robot simulators, the pipeline should be able to solve increasingly challenging robot design problems and discover more complicated shape–controller pairs. While the sim2real transfer reported in this manuscript primarily tested intermediate shapes between two extremal shapes—a fully inflated cylinder and a flattened sheet—future robots may be able to morph between shapes embedded within a richer, but perhaps less intuitive morphospace. For example, robots could be automatically designed with a set C of N_c inflatable cores and corresponding constraining fabric outer layers. To transition between shapes, a different subset C could be inflated, yielding 2^{N_c} distinct robot morphologies. Designing more sophisticated arrangements of actuators and inflatable cores could be achieved using a multilayer evolutionary algorithm, where the material properties of robots are designed along with their physical structure and control policies[51].

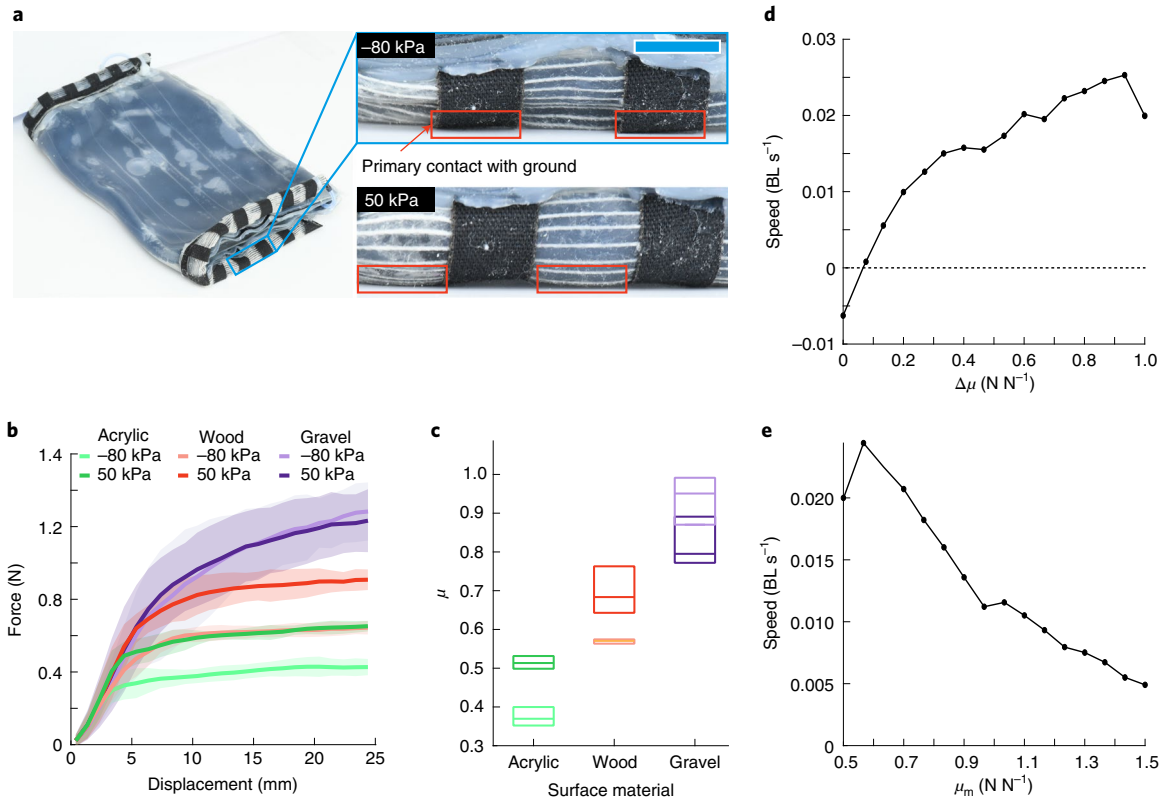

Fig. 6 | The variable-friction feet change their frictional properties when inflated. a, When the robot's feet are inflated, silicone bladders protrude from their fabric sheath to contact the ground. Blue scale bar on inset represents 1 cm. **b**, Force versus displacement when the robot was slid over wood, acrylic and gravel. Each shaded region represents ±1 s.d. about the mean (solid line). **c**, Coefficient of static friction. The boxes denote 25th and 75th percentiles, and the bars represent the median. **d**, Speed (in simulation) as a function of the difference between friction values, $\Delta\mu = \mu_i - \mu_u$ (where μ_i is friction while the foot is inflated to 50 kPa, and μ_u is friction while uninflated at −80 kPa). **e**, Speed (in simulation) as a function of average friction value, $\mu_m = (\mu_i + \mu_u)/2$. In **d** and **e**, the hand-tuned inchworm gait was used.

In addition, it is unclear how to properly embed sensors into the physical robot to measure its shape, actuator state and environment. Although some progress has been made towards intrinsically sensing the shape of soft robots[52] and environmental sensing[53], it remains an open challenge for a robot to detect that it as encountered an unforeseen environment and edit its body morphology and behavioural control policy accordingly.

Future advances in hardware and search algorithms could be used to design shape-changing robots that can operate across more challenging environmental changes. For example, swimming or amphibious robots could be automatically designed using underwater soft-robot simulation frameworks[54], and changing shape within each gait cycle might allow robots to avoid obstacles[31] or adapt to environmental transitions. We have begun extending our framework to include underwater locomotion, where locomoting between terrestrial and aquatic environments represents a more extreme environmental transition than flat-to-inclined surface environments. Our preliminary results suggest that multiple swimming shape–gait pairs can be evolved using the same pipeline and robot presented herein (Supplementary Information). While recent work has shown the potential advantages of adapting robot limb shape and gait for amphibious locomotion[55], closing the sim2real gap on shape-changing amphibious robots remains largely unstudied.

Collectively, this work represents a step towards the closed-loop automated design of robots that dynamically adjust their shape to expand their competencies. By leveraging soft materials, such robots potentially could metamorphose to attain multiple grasping modalities, adapt their dynamics to intelligently interact with their environment and change gaits to continue operation in widely different environments.

Methods

Simulation environment. The robots were simulated with the multi-material soft-robot simulator Voxelyze[34], which represents robots as a collection of cubic elements called voxels. A robot can be made to move via external forces or through expansion of a voxel along one or more of its three dimensions.

Voxels were instantiated as a lattice of Euler–Bernoulli beams (Supplementary Fig. 1a). Thus, adjacent voxels were represented as points connected by beams (Supplementary Fig. 1b). Each beam had length $l = 0.01$ m, elastic modulus $E = 400$ kPa, density $\rho = 3{,}000\,\mathrm{kg\,m^{-3}}$, coefficient of friction $\mu = 0.\overline{6}$ and damping coefficient $\zeta = 1.0$ (critically damped). For comparison, silicone typically has a modulus of ~100–600 kPa and density of ~1,000 kg m^{-3}. These parameters were initially set to $E = 100$ kPa and $\rho = 1{,}000\,\mathrm{kg\,m^{-3}}$, but were iteratively changed to increase the speed and stability of the simulation while maintaining physically realistic behaviour. We simulated gravity as an external acceleration ($g = 9.80665\,\mathrm{m\,s^{-2}}$) acting on each voxel. For the flat environment, gravity was in the simulation's negative z direction. Since changing the direction of gravity is physically equivalent to and computationally simpler than rotating the floor plane, we simulated the slope by changing the direction of gravity. The robot could change shape by varying the force pushing outward, along to the interior voxels' surface normals, representing a discrete approximation of pressure (Supplementary Fig. 1c). The maximum pressure was set at 14 kPa (1.4 N per voxel) after comparison with previous results (for example, the robotic skins introduced by Shah et al. inflated their pneumatic bladders to under 20 kPa (ref. [31])) and after initial experiments with hardware revealed only 10–35 kPa was necessary. The robots' external bladders were simulated via voxel expansion such that a voxel expanded along the z-dimension of its local coordinate space at 3×10^{-4} m per simulation step and 1.5×10^{-5} m along the x dimension. Expansion in the y dimension created a bending force on the underlying skin voxels. This value was changed on a sliding scale from 1.76×10^{-4} m to 3×10^{-5} m based on the pressure of the robots' core, such that bladder expansion created minimal bending force

when the robot was inflated, simulating the expansion of physically realizable soft robots. Concretely, the y-dimension expansion was computing using a normalizing equation $(b-a)((P-P_{MIN})/(P_{MAX}-P_{MIN}))+a$ where $a=1.7$, $b=10$, P_{MAX} is the maximum outward force per voxel in the robot's core (1.4 N), P_{MIN} is the minimum outward force per voxel (0 N) and P is the current outward force per voxel. These values were adjusted iteratively, until simulated and physical robots with the same controllers exhibited similar behaviour in both the inclined and flat environments. Lastly, to prevent the robot from slipping down the hill, and to enable other non-rolling gaits, the robot was allowed to change the static and kinetic friction of its outer voxels between a low value ($\mu=1\times10^{-4}$) when inactive and high value ($\mu=2.0$) when active.

Optimization. The optimization algorithm searched over three adjustable aspects of the robots: shape (parameterized as inner bladder pressure), orientation of the robot relative to the incline and actuation sequence. The algorithm searched over a single number $p\in[0, 1.4]$ (N per voxel) for shape and $\theta\in[0°, 90°]$ for orientation (see Supplementary Fig. 3a for illustrations of each parameter). The robot's actuation sequence S over T actuation steps was represented by a binary $10\times T$ matrix where 1 corresponds to bladder expansion and 0 corresponds to bladder deflation. Each of the first eight rows corresponded to one of the inflatable bladders, and the last two rows controlled the variable-friction feet. Each column represented the actuation to occur during a discrete amount of simulation timesteps t, resulting in a total simulation length of $t\times T$. t was set such that an actuation achieved full inflation, followed by a pause for the elastic material to settle. Actuating in this manner minimizes many effects of the complex dynamics of soft materials, reducing the likelihood of the robots exploiting idiosyncrasies of the simulation environment. In this study, we used $t\approx11{,}000$ timesteps of 0.0001 s each and $T=16$ for all simulations, for a total simulation time of 17.6 s. To populate S, the algorithm searched over a set of parameters (frequency f and offset ϕ) for each of the ten actuators. Both of these parameters were kept in the range $0-T$ where in our case we set $T=16$. f determined the number of columns between successive actuator activations, where $f=0$ created a row in the actuation matrix of all 1s, $f=1$ created a row with every other column filled by a 1, $f=2$ every two columns filled by a 1, and so on. ϕ specified the number of columns before that actuator's first activation.

We optimized the parameters of shape, orientation and actuation using a hill-climber method. This method was chosen for computational efficiency, as a single robot simulation took considerable wall-clock time (approximately 2.5 min on a 2.9 GHz Intel Core i7 processor). The hill-climber algorithm needs only one robot evaluation per optimization step, in contrast to more advanced optimization algorithms that often require multiple evaluations per optimization step. The current set of parameters C was initialized to randomly generated values and evaluated in the simulation, where fitness was defined as the distance travelled over flat ground, or distance travelled up the incline. A variant V was made by mutating each of the parameters by sampling from a normal distribution centred around the current parameters of C. V was then tested in the simulation, and if it travelled farther, the algorithm replaced C with V and generated a new V. The process of generating variations, evaluating fitness and replacing the parameters was done for 200 generations. To determine the repeatability of such an algorithm, we ran 60 independent hill climbers for each of the six experiments, as described in Results.

Parallelized simulations for critical angle experiment. To enable the extensive batch of simulations used in the distance-weighted exponential natural evolutionary strategies (DX-NES[48]) trials, changes were made to the simulator that allowed it to be more stable and efficient. First, the physics simulator was updated for parallel computation of the voxel physics. This allowed us to decrease the inflation rate of the outer bladders and increase the timestep (increasing the in-simulation time from 17.6 s to approximately 70 s), while still lowering the wall-clock time per robot simulation. We also decreased the robot's elastic modulus (from 400 kPa to 300 kPa) along with the maximum pressure of the inner core. This set of improvements had the net effect of increasing the stability of the voxel–voxel interactions, while enabling a larger number of physically realistic simulations to be run. We then ran 11 independent evolutionary trials using DX-NES, each with a population size of 100 for 100 generations, for each of six different environments, placing particular emphasis on the region around where the hand-tuned rolling gait began to consistently roll backward (between 2° and 4°).

Manufacturing the physical robot. The physical robot was designed to enable transfer of function, shapes and control policies from simulation, while maximizing locomotion speed and ease of manufacture. In summary, the inner bladder was silicone (Dragon Skin 10, abbreviated here as DS10, Smooth-On Inc.), the cylindrical body was cotton dropcloth, and the outer bladders were made with a stiffer silicone (Dragon Skin 30, abbreviated here as DS30, Smooth-On Inc.) for higher force output. The variable-friction feet were made out of latex balloons, unidirectionally stretchable lamina (STAUD prepreg, described in ref. [50]) and cotton dropcloth. Complete manufacturing details follow.

First, the outer bladders were made (Supplementary Fig. 2a). Two layers of DS10 were rod coated onto a piece of polyethylene terephthalate (PET). After curing, the substrate was placed in a laser cutter (ULS 2.0), PET-side up, and an outline of the eight bladders were cut into the PET layer. The substrate was removed from the laser cutter and the PET not corresponding to the bladders (that is, the outer 'negative' region) was removed. Two layers of DS30 were rod coated onto the substrate. DS30 is stiffer than DS10, and was used to increase the outer actuators' bending force, while DS10 was used in all other layers to keep the robot flexible. Using ethanol as a loosening agent, the encased PET was then removed from all eight bladders. Finally, a layer of DS10 was cast over the bladders' DS10 side for attaching broadcloth to begin manufacturing of the inner bladder.

The inner bladder was made by first soaking cotton broadcloth (15 cm by 20 cm) with DS10, and placing it on the uncured layer on top of the outer bladders (Supplementary Fig. 2b). PET was then laid on the robot, and the inner bladder outline was lasercut into the PET. Again, the outer PET was removed, and DS10 was rod coated to complete the inner bladder. The PET was removed using ethanol and tweezers, and silicone tubing (McMaster-Carr) was inserted into each bladder and adhered with DS10.

To make the variable-friction feet, rectangular slits were lasercut into broadcloth, and unidirectionally stretchable laminate[50] was attached using Sil-Poxy (Smooth-On Inc.) (Supplementary Fig. 2c). Latex balloons were attached using Sil-Poxy, and the feet were sealed in half with Sil-Poxy to make an enclosed envelope for each foot. When at vacuum or atmospheric pressure, the fabric would contact the environment, leading to a low-friction interaction. When the feet were inflated, the silicone would contact the environment, allowing the feet to increase their friction.

Finally, the robot was assembled by attaching the feet to the main robot body using Sil-Poxy, and the robot was folded to bond the inner bladder to the bladderless half, using DS10 (Supplementary Fig. 2d).

Experiments with the physical robot. To test the robot's locomotion capabilities, we ran the physical robots through several tests on flat and inclined ground. The pressure in the robots' bladders was controlled using pneumatic pressure regulators[49]. The robots were primarily operated on wood (flat and tipped to angles up to ~15°), with additional experiments carried out on a flat acrylic surface and a flat gravel surface (Fig. 5 and Supplementary Video 1).

The variable-friction feet were assessed by pulling the robot across three materials (acrylic, wood, gravel) using a materials testing machine (Instron 3343). The robot was placed on a candidate material and dragged across the surface at 100 mm min^{-1} for 130 mm at atmospheric conditions (23 °C, 1 atm). This process was repeated ten times for each material, at two feet inflation pressures: vacuum (−80 kPa) and inflated (50 kPa). The static coefficient of friction, μ_s, was calculated by dividing the force at the upper end of the linear regime by the weight of the robot.

The robot's shape-changing speed was assessed by manually inflating and deflating the robot's inner core for 20 cycles. For each cycle, the robot body was inflated to a cylindrical shape with a line pressure of 50 kPa, and the time required to attain a diameter of ~7 cm was recorded. The body was then deflated with a line pressure of −80 kPa, and the time required to flatten to a height of ~1.2 cm was recorded.

Reporting Summary. Further information on research design is available in the Nature Research Reporting Summary linked to this article.

Data availability

The data that support the findings of this study are available from the corresponding author upon reasonable request.

Code availability

A public repository at https://doi.org/10.5281/zenodo.4067077 contains the code necessary to reproduce the soft-robot simulations.

Received: 31 March 2020; Accepted: 22 October 2020;
Published online: 30 November 2020

References

1. Jager, P. *Cebrennus* Simon, 1880 (Araneae: Sparassidae): a revisionary up-date with the description of four new species and an updated identification key for all species. *Zootaxa* **3790**, 319–356 (2014).
2. Bhanoo, S. N. A desert spider with astonishing moves. *The New York Times* D4 (2014).
3. Armour, R. H. & Vincent, J. F. V. Rolling in nature and robotics: a review. *J. Bionic Eng.* **3**, 195–208 (2006).
4. Lin, H.-T., Leisk, G. G. & Trimmer, B. GoQBot: a caterpillar-inspired soft-bodied rolling robot. *Bioinspir. Biomim.* **6**, 026007 (2011).
5. Christensen, D. J. Evolution of shape-changing and self-repairing control for the atron self-reconfigurable robot. In *Proc. 2006 IEEE International Conference on Robotics and Automation (ICRA)* 2539–2545 (IEEE, 2006).
6. Yim, M. et al. Modular self-reconfigurable robot systems [grand challenges of robotics]. *IEEE Robot. Autom. Mag.* **14**, 43–52 (2007).

7. Parrott, C., Dodd, T. J. & Groß, R. HyMod: A 3-DOF Hybrid Mobile and Self-Reconfigurable Modular Robot and its Extensions. In *Distributed Autonomous Robotic Systems* (eds. Groß, R. et al.) 401–414 (Springer, 2018).
8. Paul, C., Valero-Cuevas, F. J. & Lipson, H. Design and control of tensegrity robots for locomotion. *IEEE Trans. Robot.* **22**, 944–957 (2006).
9. Sabelhaus, A. P. et al. System design and locomotion of superball, an untethered tensegrity robot. In *2015 IEEE International Conference on Robotics and Automation (ICRA)* 2867–2873 (IEEE, 2015).
10. Sadeghi, A., Mondini, A. & Mazzolai, B. Toward self-growing soft robots inspired by plant roots and based on additive manufacturing technologies. *Soft Robot.* **4**, 211–223 (2017).
11. Miyashita, S., Guitron, S., Ludersdorfer, M., Sung, C. R. & Rus, D. An untethered miniature origami robot that self-folds, walks, swims, and degrades. In *2015 IEEE International Conference on Robotics and Automation (ICRA)* 1490–1496 (IEEE, 2015).
12. Rus, D. & Tolley, M. T. Design, fabrication and control of origami robots. *Nat. Rev. Mater.* **3**, 101–112 (2018).
13. Pfeifer, R., Lungarella, M. & Iida, F. Self-organization, embodiment, and biologically inspired robotics. *Science* **318**, 1088–1093 (2007).
14. Saranli, U., Buehler, M. & Koditschek, D. E. Rhex: a simple and highly mobile hexapod robot. *Int. J. Robot. Res.* **20**, 616–631 (2001).
15. Raibert, M., Blankespoor, K., Nelson, G. & Playter, R. BigDog, the rough-terrain quadruped robot. *IFAC Proc. Vol.* **41**, 10822–10825 (2008).
16. Kuindersma, S. et al. Optimization-based locomotion planning, estimation, and control design for the atlas humanoid robot. *Auton. Robot.* **40**, 429–455 (2016).
17. Ijspeert, A. J., Crespi, A., Ryczko, D. & Cabelguen, J.-M. From swimming to walking with a salamander robot driven by a spinal cord model. *Science* **315**, 1416–1420 (2007).
18. Li, M., Guo, S., Hirata, H. & Ishihara, H. Design and performance evaluation of an amphibious spherical robot. *Robot. Auton. Syst.* **64**, 21–34 (2015).
19. Myeong, W. C., Jung, K. Y., Jung, S. W., Jung, Y. & Myung, H. Development of a drone-type wall-sticking and climbing robot. In *2015 12th International Conference on Ubiquitous Robots and Ambient Intelligence (URAI)* 386–389 (IEEE, 2015).
20. Bachmann, R. J., Boria, F. J., Vaidyanathan, R., Ifju, P. G. & Quinn, R. D. A biologically inspired micro-vehicle capable of aerial and terrestrial locomotion. *Mech. Mach. Theory* **44**, 513–526 (2009).
21. Roderick, W. R., Cutkosky, M. R. & Lentink, D. Touchdown to take-off: at the interface of flight and surface locomotion. *Interface Focus* **7**, 20160094 (2017).
22. Korayem, M. H., Tourajizadeh, H. & Bamdad, M. Dynamic load carrying capacity of flexible cable suspended robot: robust feedback linearization control approach. *J. Intell. Robot. Syst.* **60**, 341–363 (2010).
23. Li, J., Ma, H., Yang, C. & Fu, M. Discrete-time adaptive control of robot manipulator with payload uncertainties. In *2015 IEEE International Conference on Cyber Technology in Automation, Control, and Intelligent Systems (CYBER)* 1971–1976 (IEEE, 2015).
24. Bongard, J., Zykov, V. & Lipson, H. Resilient machines through continuous self-modeling. *Science* **314**, 1118–1121 (2006).
25. Cully, A., Clune, J., Tarapore, D. & Mouret, J.-B. Robots that can adapt like animals. *Nature* **521**, 503–507 (2015).
26. Chatzilygeroudis, K., Vassiliades, V. & Mouret, J.-B. Reset-free trial-and-error learning for robot damage recovery. *Robot. Auton. Syst.* **100**, 236–250 (2018).
27. Rosendo, A., von Atzigen, M. & Iida, F. The trade-off between morphology and control in the co-optimized design of robots. *PLoS ONE* **12**, e0186107 (2017).
28. Garrad, M., Rossiter, J. & Hauser, H. Shaping behavior with adaptive morphology. *IEEE Robot. Autom. Lett.* **3**, 2056–2062 (2018).
29. Hauser, H. Resilient machines through adaptive morphology. *Nat. Mach. Intell.* **1**, 338–339 (2019).
30. Yim, S. & Sitti, M. Shape-programmable soft capsule robots for semi-implantable drug delivery. *IEEE Trans. Robot.* **28**, 1198–1202 (2012).
31. Shah, D. S., Yuen, M. C.-S., Tilton, L. G., Yang, E. J. & Kramer-Bottiglio, R. Morphing robots using robotic skins that sculpt clay. *IEEE Robot. Autom. Lett.* **4**, 2204–2211 (2019).
32. Lee, D.-Y., Kim, S.-R., Kim, J.-S., Park, J.-J. & Cho, K.-J. Origami wheel transformer: a variable-diameter wheel drive robot using an origami structure. *Soft Robot.* **4**, 163–180 (2017).
33. Kriegman, S. et al. Automated shapeshifting for function recovery in damaged robots. In *Proc. Robotics: Science and Systems* (2019).
34. Hiller, J. & Lipson, H. Dynamic simulation of soft multimaterial 3D-printed objects. *Soft Robot.* **1**, 88–101 (2014).
35. Jakobi, N., Husbands, P. & Harvey, I. Noise and the reality gap: the use of simulation in evolutionary robotics. In *European Conference on Artificial Life* (eds. Morán, F. et al.) 704–720 (Springer, 1995).
36. Lipson, H. & Pollack, J. B. Automatic design and manufacture of robotic lifeforms. *Nature* **406**, 974 (2000).
37. Koos, S., Mouret, J.-B. & Doncieux, S. The transferability approach: crossing the reality gap in evolutionary robotics. *IEEE Trans. Evol. Comput.* **17**, 122–145 (2013).
38. Bartlett, N. W. et al. A 3D-printed, functionally graded soft robot powered by combustion. *Science* **349**, 161–165 (2015).
39. Rusu, A. A. et al. Sim-to-real robot learning from pixels with progressive nets. In *Conference on Robot Learning* 262–270 (PMLR, 2017).
40. Chebotar, Y. et al. Closing the sim-to-real loop: adapting simulation randomization with real world experience. In *2019 International Conference on Robotics and Automation (ICRA)* 8973–8979 (2019).
41. Peng, X. B., Andrychowicz, M., Zaremba, W. & Abbeel, P. Sim-to-real transfer of robotic control with dynamics randomization. In *2018 IEEE International Conference on Robotics and Automation (ICRA)* 1–8 (IEEE, 2018).
42. Hwangbo, J. et al. Learning agile and dynamic motor skills for legged robots. *Sci. Robot.* **4**, eaau5872 (2019).
43. Hiller, J. & Lipson, H. Automatic design and manufacture of soft robots. *IEEE Trans. Robot.* **28**, 457–466 (2012).
44. Mitchell, M., Holland, J. H. & Forrest, S. in *Advances in Neural Information Processing Systems 6* (eds Cowan, J. D. et al.) 51–58 (Morgan-Kaufmann, 1994).
45. Booth, J. W. et al. OmniSkins: robotic skins that turn inanimate objects into multifunctional robots. *Sci. Robot.* **3**, eaat1853 (2018).
46. Felton, S. M., Tolley, M. T., Onal, C. D., Rus, D. & Wood, R. J. Robot self-assembly by folding: a printed inchworm robot. In *2013 IEEE International Conference on Robotics and Automation* 277–282 (IEEE, 2013).
47. Lee, D., Kim, S., Park, Y. & Wood, R. J. Design of centimeter-scale inchworm robots with bidirectional claws. In *2011 IEEE International Conference on Robotics and Automation* 3197–3204 (IEEE, 2011).
48. Fukushima, N., Nagata, Y., Kobayashi, S. & Ono, I. Proposal of distance-weighted exponential natural evolution strategies. In *2011 IEEE Congress of Evolutionary Computation (CEC)* 164–171 (IEEE, 2011).
49. Booth, J. W., Case, J. C., White, E. L., Shah, D. S. & Kramer-Bottiglio, R. An addressable pneumatic regulator for distributed control of soft robots. In *2018 IEEE International Conference on Soft Robotics (RoboSoft)* 25–30 (IEEE, 2018).
50. Kim, S. Y. et al. Reconfigurable soft body trajectories using unidirectionally stretchable composite laminae. *Nat. Commun.* **10**, 3464 (2019).
51. Howard, D. et al. Evolving embodied intelligence from materials to machines. *Nat. Mach. Intell.* **1**, 12–19 (2019).
52. Soter, G., Conn, A., Hauser, H. & Rossiter, J. Bodily aware soft robots: integration of proprioceptive and exteroceptive sensors. In *2018 IEEE International Conference on Robotics and Automation (ICRA)* 2448–2453 (IEEE, 2018).
53. Umedachi, T., Kano, T., Ishiguro, A. & Trimmer, B. A. Gait control in a soft robot by sensing interactions with the environment using self-deformation. *Open Sci.* **3**, 160766 (2016).
54. Corucci, F., Cheney, N., Giorgio-Serchi, F., Bongard, J. & Laschi, C. Evolving soft locomotion in aquatic and terrestrial environments: effects of material properties and environmental transitions. *Soft Robot.* **5**, 475–495 (2018).
55. Baines, R., Freeman, S., Fish, F. & Kramer, R. Variable stiffness morphing limb for amphibious legged robots inspired by chelonian environmental adaptations. *Bioinspir. Biomim.* **15**, 025002 (2020).

Acknowledgements

This work was supported by NSF EFRI award 1830870. D.S.S. was supported by a NASA Space Technology Research Fellowship (80NSSC17K0164). J.P.P. was supported by the Vermont Space Grant Consortium under NASA Cooperative Agreement NNX15AP86H.

Author contributions

J.B., R.K.-B., S.K., D.S.S. and J.P.P. conceived the project and planned the experiments. J.P.P. coded the simulation and ran the evolutionary algorithm experiments. D.S.S. and L.G.T. manufactured the robot and performed the hardware experiments. D.S.S., J.P.P., L.G.T., S.K., J.B. and R.K.-B. drafted and edited the manuscript. All authors contributed to, and agree with, the content of the final version of the manuscript.

Competing interests

The authors declare no competing interests.

Additional information

Supplementary information is available for this paper at https://doi.org/10.1038/s42256-020-00263-1.

Correspondence and requests for materials should be addressed to R.K.-B.

Peer review information *Nature Machine Intelligence* thanks the anonymous reviewers for their contribution to the peer review of this work.

Reprints and permissions information is available at www.nature.com/reprints.

Publisher's note Springer Nature remains neutral with regard to jurisdictional claims in published maps and institutional affiliations.

nature research

Corresponding author(s): Rebecca Kramer-Bottiglio

Last updated by author(s): Oct 7, 2020

Reporting Summary

Nature Research wishes to improve the reproducibility of the work that we publish. This form provides structure for consistency and transparency in reporting. For further information on Nature Research policies, see Authors & Referees and the Editorial Policy Checklist.

Statistics

For all statistical analyses, confirm that the following items are present in the figure legend, table legend, main text, or Methods section.

n/a	Confirmed	
☐	☒	The exact sample size (*n*) for each experimental group/condition, given as a discrete number and unit of measurement
☐	☒	A statement on whether measurements were taken from distinct samples or whether the same sample was measured repeatedly
☐	☒	The statistical test(s) used AND whether they are one- or two-sided *Only common tests should be described solely by name; describe more complex techniques in the Methods section.*
☐	☒	A description of all covariates tested
☐	☒	A description of any assumptions or corrections, such as tests of normality and adjustment for multiple comparisons
☐	☒	A full description of the statistical parameters including central tendency (e.g. means) or other basic estimates (e.g. regression coefficient) AND variation (e.g. standard deviation) or associated estimates of uncertainty (e.g. confidence intervals)
☐	☒	For null hypothesis testing, the test statistic (e.g. *F*, *t*, *r*) with confidence intervals, effect sizes, degrees of freedom and *P* value noted *Give P values as exact values whenever suitable.*
☒	☐	For Bayesian analysis, information on the choice of priors and Markov chain Monte Carlo settings
☒	☐	For hierarchical and complex designs, identification of the appropriate level for tests and full reporting of outcomes
☒	☐	Estimates of effect sizes (e.g. Cohen's *d*, Pearson's *r*), indicating how they were calculated

Our web collection on statistics for biologists contains articles on many of the points above.

Software and code

Policy information about availability of computer code

Data collection	For the soft robot simulations, we utilized custom scripts that used the open source physics simulator Voxelyze and publicly-available Julia packages: Cxx, Libdl, Makie, LinearAlgebra, StatsBase, Colors, Random. Our code has been published for public access at https://doi.org/10.5281/zenodo.4067077
Data analysis	Data analysis of the physical robot was performed using standard functions in MATLAB 2019b, and simulated robots were analyzed using publicly-available Julia package HypothesisTests, and using gnuplot [www.gnuplot.info].

For manuscripts utilizing custom algorithms or software that are central to the research but not yet described in published literature, software must be made available to editors/reviewers. We strongly encourage code deposition in a community repository (e.g. GitHub). See the Nature Research guidelines for submitting code & software for further information.

Data

Policy information about availability of data

All manuscripts must include a data availability statement. This statement should provide the following information, where applicable:

- Accession codes, unique identifiers, or web links for publicly available datasets
- A list of figures that have associated raw data
- A description of any restrictions on data availability

The data that support the findings of this study are available from the corresponding author upon reasonable request

Field-specific reporting

Please select the one below that is the best fit for your research. If you are not sure, read the appropriate sections before making your selection.

☐ Life sciences ☐ Behavioural & social sciences ☐ Ecological, evolutionary & environmental sciences

For a reference copy of the document with all sections, see nature.com/documents/nr-reporting-summary-flat.pdf

Life sciences study design

All studies must disclose on these points even when the disclosure is negative.

Sample size	*Describe how sample size was determined, detailing any statistical methods used to predetermine sample size OR if no sample-size calculation was performed, describe how sample sizes were chosen and provide a rationale for why these sample sizes are sufficient.*
Data exclusions	*Describe any data exclusions. If no data were excluded from the analyses, state so OR if data were excluded, describe the exclusions and the rationale behind them, indicating whether exclusion criteria were pre-established.*
Replication	*Describe the measures taken to verify the reproducibility of the experimental findings. If all attempts at replication were successful, confirm this OR if there are any findings that were not replicated or cannot be reproduced, note this and describe why.*
Randomization	*Describe how samples/organisms/participants were allocated into experimental groups. If allocation was not random, describe how covariates were controlled OR if this is not relevant to your study, explain why.*
Blinding	*Describe whether the investigators were blinded to group allocation during data collection and/or analysis. If blinding was not possible, describe why OR explain why blinding was not relevant to your study.*

Behavioural & social sciences study design

All studies must disclose on these points even when the disclosure is negative.

Study description	*Briefly describe the study type including whether data are quantitative, qualitative, or mixed-methods (e.g. qualitative cross-sectional, quantitative experimental, mixed-methods case study).*
Research sample	*State the research sample (e.g. Harvard university undergraduates, villagers in rural India) and provide relevant demographic information (e.g. age, sex) and indicate whether the sample is representative. Provide a rationale for the study sample chosen. For studies involving existing datasets, please describe the dataset and source.*
Sampling strategy	*Describe the sampling procedure (e.g. random, snowball, stratified, convenience). Describe the statistical methods that were used to predetermine sample size OR if no sample-size calculation was performed, describe how sample sizes were chosen and provide a rationale for why these sample sizes are sufficient. For qualitative data, please indicate whether data saturation was considered, and what criteria were used to decide that no further sampling was needed.*
Data collection	*Provide details about the data collection procedure, including the instruments or devices used to record the data (e.g. pen and paper, computer, eye tracker, video or audio equipment) whether anyone was present besides the participant(s) and the researcher, and whether the researcher was blind to experimental condition and/or the study hypothesis during data collection.*
Timing	*Indicate the start and stop dates of data collection. If there is a gap between collection periods, state the dates for each sample cohort.*
Data exclusions	*If no data were excluded from the analyses, state so OR if data were excluded, provide the exact number of exclusions and the rationale behind them, indicating whether exclusion criteria were pre-established.*
Non-participation	*State how many participants dropped out/declined participation and the reason(s) given OR provide response rate OR state that no participants dropped out/declined participation.*
Randomization	*If participants were not allocated into experimental groups, state so OR describe how participants were allocated to groups, and if allocation was not random, describe how covariates were controlled.*

Ecological, evolutionary & environmental sciences study design

All studies must disclose on these points even when the disclosure is negative.

Study description	*Briefly describe the study. For quantitative data include treatment factors and interactions, design structure (e.g. factorial, nested, hierarchical), nature and number of experimental units and replicates.*
Research sample	*Describe the research sample (e.g. a group of tagged Passer domesticus, all Stenocereus thurberi within Organ Pipe Cactus National*

Research sample	*Monument), and provide a rationale for the sample choice. When relevant, describe the organism taxa, source, sex, age range and any manipulations. State what population the sample is meant to represent when applicable. For studies involving existing datasets, describe the data and its source.*
Sampling strategy	*Note the sampling procedure. Describe the statistical methods that were used to predetermine sample size OR if no sample-size calculation was performed, describe how sample sizes were chosen and provide a rationale for why these sample sizes are sufficient.*
Data collection	*Describe the data collection procedure, including who recorded the data and how.*
Timing and spatial scale	*Indicate the start and stop dates of data collection, noting the frequency and periodicity of sampling and providing a rationale for these choices. If there is a gap between collection periods, state the dates for each sample cohort. Specify the spatial scale from which the data are taken*
Data exclusions	*If no data were excluded from the analyses, state so OR if data were excluded, describe the exclusions and the rationale behind them, indicating whether exclusion criteria were pre-established.*
Reproducibility	*Describe the measures taken to verify the reproducibility of experimental findings. For each experiment, note whether any attempts to repeat the experiment failed OR state that all attempts to repeat the experiment were successful.*
Randomization	*Describe how samples/organisms/participants were allocated into groups. If allocation was not random, describe how covariates were controlled. If this is not relevant to your study, explain why.*
Blinding	*Describe the extent of blinding used during data acquisition and analysis. If blinding was not possible, describe why OR explain why blinding was not relevant to your study.*

Did the study involve field work? ☐ Yes ☐ No

Field work, collection and transport

Field conditions	*Describe the study conditions for field work, providing relevant parameters (e.g. temperature, rainfall).*
Location	*State the location of the sampling or experiment, providing relevant parameters (e.g. latitude and longitude, elevation, water depth).*
Access and import/export	*Describe the efforts you have made to access habitats and to collect and import/export your samples in a responsible manner and in compliance with local, national and international laws, noting any permits that were obtained (give the name of the issuing authority, the date of issue, and any identifying information).*
Disturbance	*Describe any disturbance caused by the study and how it was minimized.*

Reporting for specific materials, systems and methods

We require information from authors about some types of materials, experimental systems and methods used in many studies. Here, indicate whether each material, system or method listed is relevant to your study. If you are not sure if a list item applies to your research, read the appropriate section before selecting a response.

Materials & experimental systems

n/a	Involved in the study
☐	☐ Antibodies
☐	☐ Eukaryotic cell lines
☐	☐ Palaeontology
☐	☐ Animals and other organisms
☐	☐ Human research participants
☐	☐ Clinical data

Methods

n/a	Involved in the study
☐	☐ ChIP-seq
☐	☐ Flow cytometry
☐	☐ MRI-based neuroimaging

Antibodies

Antibodies used	*Describe all antibodies used in the study; as applicable, provide supplier name, catalog number, clone name, and lot number.*
Validation	*Describe the validation of each primary antibody for the species and application, noting any validation statements on the manufacturer's website, relevant citations, antibody profiles in online databases, or data provided in the manuscript.*

Eukaryotic cell lines

Policy information about cell lines

Cell line source(s)	*State the source of each cell line used.*
Authentication	*Describe the authentication procedures for each cell line used OR declare that none of the cell lines used were authenticated.*
Mycoplasma contamination	*Confirm that all cell lines tested negative for mycoplasma contamination OR describe the results of the testing for mycoplasma contamination OR declare that the cell lines were not tested for mycoplasma contamination.*
Commonly misidentified lines (See ICLAC register)	*Name any commonly misidentified cell lines used in the study and provide a rationale for their use.*

Palaeontology

Specimen provenance	*Provide provenance information for specimens and describe permits that were obtained for the work (including the name of the issuing authority, the date of issue, and any identifying information).*
Specimen deposition	*Indicate where the specimens have been deposited to permit free access by other researchers.*
Dating methods	*If new dates are provided, describe how they were obtained (e.g. collection, storage, sample pretreatment and measurement), where they were obtained (i.e. lab name), the calibration program and the protocol for quality assurance OR state that no new dates are provided.*

☐ Tick this box to confirm that the raw and calibrated dates are available in the paper or in Supplementary Information.

Animals and other organisms

Policy information about studies involving animals; ARRIVE guidelines recommended for reporting animal research

Laboratory animals	*For laboratory animals, report species, strain, sex and age OR state that the study did not involve laboratory animals.*
Wild animals	*Provide details on animals observed in or captured in the field; report species, sex and age where possible. Describe how animals were caught and transported and what happened to captive animals after the study (if killed, explain why and describe method; if released, say where and when) OR state that the study did not involve wild animals.*
Field-collected samples	*For laboratory work with field-collected samples, describe all relevant parameters such as housing, maintenance, temperature, photoperiod and end-of-experiment protocol OR state that the study did not involve samples collected from the field.*
Ethics oversight	*Identify the organization(s) that approved or provided guidance on the study protocol, OR state that no ethical approval or guidance was required and explain why not.*

Note that full information on the approval of the study protocol must also be provided in the manuscript.

Human research participants

Policy information about studies involving human research participants

Population characteristics	*Describe the covariate-relevant population characteristics of the human research participants (e.g. age, gender, genotypic information, past and current diagnosis and treatment categories). If you filled out the behavioural & social sciences study design questions and have nothing to add here, write "See above."*
Recruitment	*Describe how participants were recruited. Outline any potential self-selection bias or other biases that may be present and how these are likely to impact results.*
Ethics oversight	*Identify the organization(s) that approved the study protocol.*

Note that full information on the approval of the study protocol must also be provided in the manuscript.

Clinical data

Policy information about clinical studies

All manuscripts should comply with the ICMJE guidelines for publication of clinical research and a completed CONSORT checklist must be included with all submissions.

Clinical trial registration	*Provide the trial registration number from ClinicalTrials.gov or an equivalent agency.*
Study protocol	*Note where the full trial protocol can be accessed OR if not available, explain why.*
Data collection	*Describe the settings and locales of data collection, noting the time periods of recruitment and data collection.*

Outcomes — *Describe how you pre-defined primary and secondary outcome measures and how you assessed these measures.*

ChIP-seq

Data deposition

☐ Confirm that both raw and final processed data have been deposited in a public database such as GEO.

☐ Confirm that you have deposited or provided access to graph files (e.g. BED files) for the called peaks.

Data access links
May remain private before publication.
For "Initial submission" or "Revised version" documents, provide reviewer access links. For your "Final submission" document, provide a link to the deposited data.

Files in database submission — *Provide a list of all files available in the database submission.*

Genome browser session
(e.g. UCSC)
Provide a link to an anonymized genome browser session for "Initial submission" and "Revised version" documents only, to enable peer review. Write "no longer applicable" for "Final submission" documents.

Methodology

Replicates — *Describe the experimental replicates, specifying number, type and replicate agreement.*

Sequencing depth — *Describe the sequencing depth for each experiment, providing the total number of reads, uniquely mapped reads, length of reads and whether they were paired- or single-end.*

Antibodies — *Describe the antibodies used for the ChIP-seq experiments; as applicable, provide supplier name, catalog number, clone name, and lot number.*

Peak calling parameters — *Specify the command line program and parameters used for read mapping and peak calling, including the ChIP, control and index files used.*

Data quality — *Describe the methods used to ensure data quality in full detail, including how many peaks are at FDR 5% and above 5-fold enrichment.*

Software — *Describe the software used to collect and analyze the ChIP-seq data. For custom code that has been deposited into a community repository, provide accession details.*

Flow Cytometry

Plots

Confirm that:

☐ The axis labels state the marker and fluorochrome used (e.g. CD4-FITC).

☐ The axis scales are clearly visible. Include numbers along axes only for bottom left plot of group (a 'group' is an analysis of identical markers).

☐ All plots are contour plots with outliers or pseudocolor plots.

☐ A numerical value for number of cells or percentage (with statistics) is provided.

Methodology

Sample preparation — *Describe the sample preparation, detailing the biological source of the cells and any tissue processing steps used.*

Instrument — *Identify the instrument used for data collection, specifying make and model number.*

Software — *Describe the software used to collect and analyze the flow cytometry data. For custom code that has been deposited into a community repository, provide accession details.*

Cell population abundance — *Describe the abundance of the relevant cell populations within post-sort fractions, providing details on the purity of the samples and how it was determined.*

Gating strategy — *Describe the gating strategy used for all relevant experiments, specifying the preliminary FSC/SSC gates of the starting cell population, indicating where boundaries between "positive" and "negative" staining cell populations are defined.*

☐ Tick this box to confirm that a figure exemplifying the gating strategy is provided in the Supplementary Information.

Magnetic resonance imaging

Experimental design

Design type	*Indicate task or resting state; event-related or block design.*
Design specifications	*Specify the number of blocks, trials or experimental units per session and/or subject, and specify the length of each trial or block (if trials are blocked) and interval between trials.*
Behavioral performance measures	*State number and/or type of variables recorded (e.g. correct button press, response time) and what statistics were used to establish that the subjects were performing the task as expected (e.g. mean, range, and/or standard deviation across subjects).*

Acquisition

Imaging type(s)	*Specify: functional, structural, diffusion, perfusion.*
Field strength	*Specify in Tesla*
Sequence & imaging parameters	*Specify the pulse sequence type (gradient echo, spin echo, etc.), imaging type (EPI, spiral, etc.), field of view, matrix size, slice thickness, orientation and TE/TR/flip angle.*
Area of acquisition	*State whether a whole brain scan was used OR define the area of acquisition, describing how the region was determined.*

Diffusion MRI ☐ Used ☐ Not used

Preprocessing

Preprocessing software	*Provide detail on software version and revision number and on specific parameters (model/functions, brain extraction, segmentation, smoothing kernel size, etc.).*
Normalization	*If data were normalized/standardized, describe the approach(es): specify linear or non-linear and define image types used for transformation OR indicate that data were not normalized and explain rationale for lack of normalization.*
Normalization template	*Describe the template used for normalization/transformation, specifying subject space or group standardized space (e.g. original Talairach, MNI305, ICBM152) OR indicate that the data were not normalized.*
Noise and artifact removal	*Describe your procedure(s) for artifact and structured noise removal, specifying motion parameters, tissue signals and physiological signals (heart rate, respiration).*
Volume censoring	*Define your software and/or method and criteria for volume censoring, and state the extent of such censoring.*

Statistical modeling & inference

Model type and settings	*Specify type (mass univariate, multivariate, RSA, predictive, etc.) and describe essential details of the model at the first and second levels (e.g. fixed, random or mixed effects; drift or auto-correlation).*
Effect(s) tested	*Define precise effect in terms of the task or stimulus conditions instead of psychological concepts and indicate whether ANOVA or factorial designs were used.*

Specify type of analysis: ☐ Whole brain ☐ ROI-based ☐ Both

Statistic type for inference (See Eklund et al. 2016)	*Specify voxel-wise or cluster-wise and report all relevant parameters for cluster-wise methods.*
Correction	*Describe the type of correction and how it is obtained for multiple comparisons (e.g. FWE, FDR, permutation or Monte Carlo).*

Models & analysis

n/a	Involved in the study
☐	☐ Functional and/or effective connectivity
☐	☐ Graph analysis
☐	☐ Multivariate modeling or predictive analysis

Functional and/or effective connectivity	*Report the measures of dependence used and the model details (e.g. Pearson correlation, partial correlation, mutual information).*
Graph analysis	*Report the dependent variable and connectivity measure, specifying weighted graph or binarized graph, subject- or group-level, and the global and/or node summaries used (e.g. clustering coefficient, efficiency, etc.).*

Multivariate modeling and predictive analysis

Specify independent variables, features extraction and dimension reduction, model, training and evaluation metrics.